HHS Public Access

Author manuscript

Phys Med Biol. Author manuscript; available in PMC 2018 May 07.

Published in final edited form as:

Phys Med Biol. 2017 May 07; 62(9): 3440–3453. doi:10.1088/1361-6560/aa5f48.

Tracking short-term biodistribution and long-term clearance of SPIO tracers in Magnetic Particle Imaging

Paul Keselman[1], **Elaine Y. Yu**[1], **Xinyi Y. Zhou**[1], **Patrick W. Goodwill**[3], **Prashant Chandrasekharan**[1], **R. Matthew Ferguson**[4], **Amit P. Khandhar**[4], **Scott J. Kemp**[4], **Kannan M. Krishnan**[4,5], **Bo Zheng**[1], and **Steven M. Conolly**[1,2]

[1]Department of Bioengineering, University of California Berkeley, Berkeley CA 94720

[2]Department of Electrical Engineering and Computer Sciences, University of California Berkeley Berkeley CA 94720

[3]Magnetic Insight Inc., Newark CA 94560

[4]LodeSpin Labs, PO Box 95632, Seattle WA 98145

[5]Department of Material Science and Engineering, University of Washington, Seattle WA 98195

Abstract

Magnetic Particle Imaging (MPI) is an emerging tracer-based medical imaging modality that images non-radioactive, kidney-safe superparamagnetic iron oxide (SPIO) tracers. MPI offers quantitative, high-contrast and high-SNR images, so MPI has exceptional promise for applications such as cell tracking, angiography, brain perfusion, cancer detection, traumatic brain injury and pulmonary imaging. In assessing MPI's utility for applications mentioned above, it is important to be able to assess tracer short-term biodistribution as well as long-term clearance from the body. Here, we describe the biodistribution and clearance for two commonly used tracers in MPI: Ferucarbotran (Meito Sangyo Co., Japan) and LS-oo8 (LodeSpin Labs, Seattle, WA). We successfully demonstrate that 3D MPI is able to quantitatively assess short-term biodistribution, as well as long-term tracking and clearance of these tracers *in vivo*.

1. Introduction

Magnetic Particle Imaging (MPI) is an emerging tracer-based medical imaging modality that images non-radioactive, kidney-safe superparamagnetic iron oxide (SPIO) tracers (Gleich and Weizenecker 2005; Saritas et al. 2013; Goodwill and Conolly 2010). Unlike iodinated contrast agents used in X-ray based modalities, or gadolinium contrast agents used in Magnetic Resonance Imaging (MRI), SPIOs are cleared through the liver and spleen instead of the kidneys, so MPI may be safer for patients with the common condition Chronic Kidney Disease (Gu et al. 2012). As with other tracer modalities such as positron emission tomography (PET) and single photon emission computed tomography (SPECT), only the tracer produces signal. There is no inherent signal from the background tissue, unless the tracer is metabolized in that tissue. This is ideal for contrast but nonspecific uptake can occur with any tracer modality. As one example, PET studies often show nonspecific activity in the bladder. A potential advantage of MPI is improved safety since it uses safe low frequency magnetic fields with no ionizing radiation. Also, another potential advantage of

MPI is that no attenuation correction is needed to render the images quantitative, since the signal suffers zero tissue attenuation. As long as the tracer does not aggregate, the MPI signal is linear and quantitative with the amount of tracer in each pixel at any tissue depth (Lu et al. 2013; Zheng et al. 2015; Zheng et al. 2016; Goodwill et al. 2012). Also, SPIO tracers remain magnetic indefinitely, so there are no tradeoffs between contrast and tracer half-life — a significant concern in Nuclear Medicine. MPI has great sensitivity. Recently, Zheng et al. (Zheng et al. 2015) reported a detection limit of 200 SPIO labeled cells with MPI (scan time: 20 s), in comparison MRI has a sensitivity of about 10^4 cells (acquisition time: minutes to hours) (Nguyen, Riegler, and Wu 2014). A similar number for sensitivity in MRI was recently reported by Chehade et al (Chehade, Srivastava, and J. W. M. Bulte 2016). Prototype MPI scanners report roughly 200 nM iron sensitivity (Zheng et al. 2015; Zheng et al. 2016), and optimization of hardware and SPIOs could still improve on this sensitivity.

The SPIOs typically used in MPI are single-domain iron oxide nanoparticles (Fe_3O_4) with a core diameter of roughly 15–35 nm. These nanoparticles are coated (and sometimes functionalized), extending their hydrodynamic radius to roughly 100 nm. Some commonly used coatings include dextran, cyclodextran and polyethylene glycol (PEG) (Ferguson et al. 2011).

Due to its zero-radiation and high contrast-to-noise ratio, MPI shows great promise for applications such as cell tracking (Zheng et al. 2015; Zheng et al. 2016), angiography (Rahmer et al. 2013), brain perfusion (Goodwill et al. 2015), traumatic brain injury (Orendorff et al. 2016) and pulmonary imaging (Zhou et al. 2016). Since MPI images nanoscale-sized SPIO nanoparticles, it may be highly useful for visualizing the delivery of nanomedicine therapeutics *in vivo*. For example, MPI may be useful for monitoring of magnetic hyperthermia, which uses similarly-sized SPIO nanoparticles for non-invasive treatment of tumors (Dutz and Hergt 2014; Hergt et al. 2006; Shinkai 2002). Nanomedicine researchers have also used SPIOs for tracking the efficacy of drug delivery (e.g., through liposomal or nebulized methods) via MRI (Allen and Cullis 2013; O'Callaghan and Barry 1997; Li et al. 2012). Also, since SPIOs are readily taken up by a wide variety of cells, they have been used in both immune cell tracking with MRI (Ahrens and J. Bulte 2013) and stem cell tracking with MPI (Zheng et al. 2015; Zheng et al. 2016). Last, MPI and MRI imaging of SPIOs have found use in cancer imaging, both through the use of targeted particles and through the enhanced permeability and retention (EPR) effect (Yu et al. 2016; Maeda, Nakamura, and Fang 2013).

For many of the applications mentioned above, it will be crucial to fully understand the normal blood circulation time and the kinetics and biodistribution of SPIO clearance. These metrics will help SPIO nanoparticle experts to optimize coatings tailoring for specific applications. For example, achieving adequate circulation time is crucial for SPIOs tailored to applications such as cardiovascular, stroke and tumor imaging (Jokerst et al. 2011; Ferguson et al. 2015). Understanding and achieving long-term clearance is crucial for applications such as tracking extended release therapeutics and cell behavior over time.

Here, we show that 3D MPI allows for quantitative measurements of SPIO blood circulation and organ distribution kinetics for up to 70 days. In particular, we demonstrate these 3D MPI

measurements for two commonly used tracers in MPI: Ferucarbotran (Meito Sangyo Co., Japan) and LS-oo8 (LodeSpin Labs, Seattle, WA). We successfully demonstrate that MPI is able to quantitatively assess short-term biodistribution as well as long-term biodistribution and clearance of these tracers *in vivo*.

2. Materials and Methods

2.1. SPIO Tracers

Ferucarbotran is an aqueous suspension of multi-core carboxydextran-coated magnetite nanoparticles, originally designed as a liver-targeting MRI contrast agent (Abdollah et al. 2014), and adopted for use in MPI (Lüdtke-Buzug et al. 2009; Ferguson et al. 2013). LS-008 is a PEG-coated single-core magnetite nanoparticle, designed as a long circulating MPI tracer (Ferguson et al. 2015; Kemp et al. 2016; Ferguson et al. 2013). Chemical structures of the tracer coatings are shown in Figure 1. In addition, characteristics for each tracer are summarized in Table 1

2.2. Tracer Linearity

To measure the linearity of each tracer in MPI, a series of seven 1 μl sources were prepared for both LS-008 and Ferucarbotran. For LS-008, the concentrations imaged were 0.08 mg/ml, 0.04 mg/ml, 0.07 mg/ml, 0.15 mg/ml, 0.29 mg/ml, 0.59 mg/ml, and 1.18 mg/ml. For Ferucarbotran, the concentrations imaged were 0.04 mg/ml, 0.09 mg/ml, 0.18 mg/ml, 0.36 mg/ml, 0.71 mg/ml, 1.43 mg/ml, and 2.85 mg/ml.

2.3. Experimental Setup

Six groups of Fisher 344 female rats were used for the biodistribution and clearance experiments. Three of the six groups were imaged over 70 days and then euthanized, and three of the six groups were imaged over 2 days and then euthanized. This was done to confirm the early and late time point localization of tracer with *ex vivo* imaging of separate organs. The first group (n = 3, weight = 134 g ± 5 g, 10 weeks old) received an injection of Ferucarbotran, and was imaged over 70 days. The second group (n = 3, weight = 117 g ± 3 g, 8 weeks old) received an injection of Ferucarbotran, and was imaged over 2 days. The third group (n = 3, weight 131 g ± 6 g, 9 weeks old) received an injection of LS-008, and was imaged over 70 days. The fourth group (n = 3, weight = 119 g ± 8 g, 8 weeks old) received an injection of LS-008, and was imaged over 2 days. The fifth group (n = 2, weight = 157 g ± 4 g, 20 weeks old) received no injection, and was imaged for 70 days. Finally, the sixth group (n = 3, weight = 116 g ± 5 g, 8 weeks old) received no injection, and was imaged for 2 days. Figure 2 is a flow chart describing the experiment.

Prior to all procedures, animals were anesthetized with an isoflurane/oxygen mixture (induction at 3.5% isoflurane and 1 L/min flow; maintenance at 2-3% isoflurane and 1 L/min flow). For groups 1, 2, 3 and 4, the tracer was diluted in sterile 0.9% saline solution, and then injected through a catheter as a bolus at a dose of 5 mg Fe/kg into the tail vein of the animal. To ensure complete delivery of the tracer, the catheter lines were flushed with 0.9% saline solution up to a total injected volume of 1 ml. All animal experiments were performed in compliance with the Animal Care and Use Committee at UC Berkeley.

2.4. Imaging Hardware

The rats were imaged with respiratory gating (SA Instruments Inc., Stony Brook, NY, USA) using a 3.5 T/m × 3.5 T/m × 7 T/m field free point MPI imager (Goodwill et al. 2012) with a 20.025 kHz and 40 mTpp excitation field in z, and field-of-view (FOV) of 4.0 cm × 4.0 cm × 10.5 cm. The animals were positioned in dorsal recumbency for imaging. For Groups 1 and 3, the animals were imaged at 10 minutes, 30 minutes, 1 hour, 2 hours, 4 hours, 6 hours, 12 hours, 1 day and 2 days and then twice a week over the next 70 days. For Groups 2 and 4, the animals were imaged right after the injection and then again at day 2. For Group 5, the animals were imaged at day 70. For Group 6, the animals were imaged at day 2.

To provide an anatomical reference for MPI images, a planar X-ray image of each animal was also acquired on a Kubtec XPERT 40 specimen radiography system. (KUB Technologies, Inc., Medford, CT, USA) immediately following the last MPI time point.

2.5. Image Reconstruction and Clearance Calculations

MPI images were reconstructed using an x-space reconstruction technique (Goodwill and Conolly 2010; Goodwill and Conolly 2011; Lu et al. 2013) with optimized DC recovery (Lu et al. 2013; Konkle et al. 2014), partial field of view overlap set at 20%, and employing an equalization filter (Lu et al. 2015).

All image analysis were performed with MATLAB Release 2016b (The MathWorks, Inc., Natick, MA, USA). First, a region growing algorithm, seeded with the maximum voxel and set to terminate at 10% of maximum, was used to draw a region of interest (ROI) around each organ in question. The half-life was then calculated by using a nonlinear least-squares 1st order exponential fit to the average value in the ROI over all animals at each time point.

2.6. Iron Localization with ex vivo MPI

Following the last time point, all animals were euthanized via an overdose of isoflurane. Liver, spleen, kidneys, lungs and heart were removed and imaged in the MPI scanner using the same imaging parameters as used for *in vivo* imaging. The same region growing algorithm was used to calculate the average signal in each organ. Control animals were also imaged to insure that there was no detectable signal from native iron in each organ.

3. Results

3.1. Tracer Linearity

Figure 3 is a photograph of the point source phantom and the corresponding maximum projection intensity MPI image as well as the plot of MPI signal versus Fe concentration for both LS-008 and Ferucarbotran. MPI signal for both tracers is linear with concentration (R^2 = 0.99 for both LS-008 and Ferucarbotran).

3.2. Blood Half-Life

To assess the blood half-life of each tracer, the jugular vein of each animal at each time point up to 48 hours was isolated in the MPI images using the method described above. The ROI over the jugular was 46 ± 7 μl. Figure 4 show coronal maximum intensity projection MPI

images of the biodistribution for both tracers overlaid onto an X-ray projection image at representative time points. Note that all MPI images shown in this paper are maximum intensity projections of the 3D MPI imaging volume. Figure 5 shows MPI signal in blood over time for both tracers over 48 hours along with corresponding exponential fits. Ferucarbotran immediately cleared out of the bloodstream, so no fit was performed. LS-008 particles persisted in the bloodstream of the rats with a half-life of 4.2 h ± 0.5 h. No MPI signal above the interference noise floor was detected in the control animals. The drastic difference in biodistribution for the two tracers is clearly captured by MPI.

3.3. Long-term Clearance

A similar algorithm to the one used to measure the blood half-life was used to assess the clearance half-life in both liver and spleen of each rat. Average signal in both organs was determined for all time points over the 70-day period. Figure 6 show coronal MPI images of a rat injected with Ferucarbotran and LS-008 tracers overlaid on X-Ray projection images. Figure 7 shows the corresponding iron clearance of Ferucarbotran and LS-008 from the liver and spleen over a 70-day period. Ferucarbotran predominantly clears through the liver, while LS-008 clears through the spleen.

Ferucarbotran cleared from the liver with a half-life of 5.6 d ± 0.2 d and from the spleen with a half-life of 4.0 d ± 0.5 d. LS-008 cleared from the liver with a half-life of 6.5 d ± 0.7 d and from the spleen with a half-life of 18.2 d ± 2.5 d. Again, no signal above the interference noise floor was detected from the liver and spleen of the control animals.

3.4. Iron Localization with ex vivo MPI

To validate the localization of the tracer with *in vivo* MPI, the heart, lungs, liver, spleen and kidneys of each rat were extracted and imaged *ex vivo* with MPI. Figure 8(a) is a photograph of the extracted organs. For both tracers, only the liver and spleen were visible in MPI at day 2 (Figure 8(b) and (d)). At day 70, LS-008 was only visible in the spleen (Figure 8(c)), and Ferucarbotran was only visible in the liver (Figure 8(e)). Using the same region growing algorithm, an average signal was determined in an ROI drawn over liver and spleen and an average signal per gram of tissue was determined. Results are shown in Figure 9.

4. Discussion

MPI signal has already been validated with Inductively Coupled Plasma measurements to correspond to injected iron content (Zheng et al. 2016). This makes MPI a powerful and quantitative tool for studying tracer dynamics *in vivo* without the need for blood draws or organ extractions.

As expected, in animals injected with the liver-targeting agent, Ferucarbotran, most of the tracer cleared into the liver immediately following the injection. On the other hand, the LS-008 particles persisted in the blood for several hours after the injection and then cleared into the spleen. This is especially exciting for MPI in applications such as angiography (Wang et al. 2015), cancer imaging (Bae, Mrsny, and Park 2013) or theraputic applications (Janib, Moses, and MacKay 2010) where long circulation time is beneficial.

In MRI the most widely used blood pool imaging agent is a gadolinium chelate, gadofosveset trisodium which allows for an imaging window of about 20 minutes in humans (Ruangwattanapaisarn, Hsiao, and Vasanawala 2015). Another, and one that is most closely comparable to tracers used in MPI, is Ferumoxytol. Ferumoxytol is an SPIO-based blood pool agent which, in humans, has a circulating half-life of about 14 hours (ibid.) and provides a good blood vessel to myocardium contrast ratio of about 3 (ibid.). In comparison, in this study we were able to achieve a blood circulation half-life of about 4 hours and a contrast to background ratio of about 2.5 as seen in Figure 4. This should be sufficient for angiography, and should only get better with improvements in hardware and further tailoring of the SPIO particles.

The *ex vivo* MPI data shown in Figure 9 confirms that both of the SPIO tracers were cleared into the liver and spleen of the animals, with no detectable iron remaining in other major organs. This agrees with *in vivo* MPI data shown in Figure 7. This was expected since MPI is quantitative with no tissue attenuation and confirms the potential of MPI to become a powerful non-invasive, quantitative imaging tool.

As mentioned before, Ferucarbotran is an aqueous solution of magnetite similar to that manufactured by Bayer under the trade name Resovist (SH U555A). Lawaczeck et al. (Lawaczeck et al. 1997), reported a circulating half-life for Resovist of about 6 minutes in rats and a liver half-life of about 5 days after injection of 100 um/kg (5.6 mg/kg). Although, we were not able to confirm blood circulation half-life of resovist due to current hardware limitations, our result of liver clearance half-life of 5.6 days agrees to that reported by Lawaczeck et al.

It is also important to note that there are other approaches to increasing blood circulation half-life. For example the approach taken by Antonelli et al. (Antonelli, Sfara, Battistelli, et al. 2013; Antonelli, Sfara, Weber, et al. 2016) of loading SPIO nanoparticles in red blood cells (RBCs). Antonelli et al were able to achieve a blood circulation half-life of 48 hours for Resovist loaded RBCs. They have also found, that similar to LS-008 particles, the Resovist loaded RBCs were mostly cleared through the spleen. It will be intriguing to see how Resovist loaded RBC would perform in our custom made MPI scanners.

We have shown two different SPIO nanoparticle tracers with very different biodistribution kinetics and clearance dynamics. In developing new SPIO tracers, one will have to tailor and optimize the nanoparticle to fit the intended application. For example, specific applications must balance imaging resolution (angiography versus oncology), tracer blood half-life (liver imaging which doesn't depend on long circulating particles vs angiography, perfusion imaging and cancer which might need multiple passes of SPIO over the region of interest to be more effective), tracer coating thickness and/or binding (to bind to stem cells, amyloid plaques or tumors), different relaxation behaviors (for color-contrast MPI (Rahmer et al. 2015; Hensley et al. 2015)), and so on. This study shows that 3D MPI can help to optimize tailored-SPIO tracers for specific applications.

With this experiment we have successfully demonstrated that MPI is able to track both short-term biodistribution and long-term clearance of SPIO particles. We confirmed that

Ferucarbotran tracer cleared directly to the liver, which would make it a great tracer for imaging the liver — as intended. On the other hand, because LS-008 SPIO particles stayed in the blood stream significantly longer than Ferucarbotran, we were able to image vasculature *in vivo*. This makes MPI a promising tool for applications that require longer circulation times such as angiography, traumatic brain injury, stroke and tumor imaging. The difference in clearance mechanisms between the two particles could be related to several characteristics. Nanoparticle size, shape and surface charge dictate biodistribution among the different organs as well as overall clearance rate from the body (Blanco, Shen, and Ferrari 2015).

One possible concern would be a significant amount of tracer remaining in the liver and spleen for several weeks after the injection. Both tracers lingered in the system before being cleared. However, several SPIOs have already been approved for human use in both US and Europe (Wang 2011) and other studies have found SPIOs to be non-toxic in the short-term (specific to particular dosage and functionalization) (Mahmoudi et al. 2012).

It is intriguing, and should be a subject of further research, that Ferucarbotran was mostly cleared by the liver while LS-008 was mostly cleared by the spleen. As mentioned previously this might be due to the difference in particle shape, size and surface charge. It would also be useful to understand if it would be possible to create a particle with a long half-life in the blood while retaining a fast clearance half-life in the liver and spleen. This would make it possible to do back-to-back injections of these SPIOs for repeated imaging studies (Mahmoudi et al. 2012).

5. Conclusion

MPI's ability to quantitatively assess particle concentration *in vivo* make it a powerful tool with many possible applications in fields of stem cell therapies, coronary artery disease, traumatic brain injury and cancer. The development of tailored particles — whether for long circulation time, for organ-specific targeting, or high resolution imaging — is crucial for these applications. Here, we were able to successfully track both the short-term biodistribution as well as long-term clearance of two tracers with MPI. This work serves as a stepping stone for the *in vivo* evaluation of these emerging particles by assessing two fundamental nanoparticle properties, organ biodistribution and clearance time.

Acknowledgments

We are grateful for funding support from the Keck Foundation Grant 009323, NIH 1R01EB019458, NIH 1R24MH106053, NIH 2R42EB013520-02A1, and the UC Discovery Grant.

References

Abdollah, Maha R., et al. Prolonging the circulatory retention of SPIONs using dextran sulfate: in vivo tracking achieved by functionalisation with near-infrared dyes. Faraday discussions. 2014; 00:1–18. url: http://www.ncbi.nlm.nih.gov/pubmed/25298115. DOI: 10.1039/c4fd00114a

Ahrens, Eric, Bulte, Jeff. Tracking immune cells in vivo using magnetic resonance imaging. Nature reviews Immunology. 2013; 13(10):755–63. url: http://dx.doi.org/10.1038/nri3531. DOI: 10.1038/nri3531

Allen, Theresa M., Cullis, Pieter R. Liposomal drug delivery systems: From concept to clinical applications. Advanced Drug Delivery Reviews. 2013; 65(1):36–48. url: http://dx.doi.org/10.1016/j.addr.2012.09.037. DOI: 10.1016/j.addr.2012.09.037 [PubMed: 23036225]

Antonelli, Antonella, Sfara, Carla, Battistelli, Serafina, Canonico, Barbara, Arcangeletti, Marcella, Manuali, Elisabetta, Salamida, Sonia, Papa, Stefano, Magnani, Mauro. Louie, Angelique, editor. New Strategies to Prolong the In Vivo Life Span of Iron-Based Contrast Agents for MRI; PLoS ONE. 2013. p. e78542url: http://dx.plos.org/10.1371/journal.pone.0078542

Antonelli, Antonella, Sfara, Carla, Weber, Oliver, Pison, Ulrich, Manuali, Elisabetta, Salamida, Sonia, Magnani, Mauro. Characterization of ferucarbotran-loaded RBCs as long circulating magnetic contrast agents. Nanomedicine. 2016; 11 nnm–2016–0216. url: http://www.futuremedicine.com/doi/10.2217/nnm-2016-0216. doi: 10.2217/nnm-2016-0216

Bae, You Han, Mrsny, Randall J., Park, Kinam. Cancer Targeted Drug Delivery: An Elusive Dream. Springer Science and Business Media; 2013.

Blanco, Elvin, Shen, Haifa, Ferrari, Mauro. Principles of nanoparticle design for overcoming biological barriers to drug delivery. Nat Biotech. 2015; 33(9):941–951. url: http://dx.doi.org/10.1038/nbt.3330%20http://10.1038/nbt.3330.

Chehade, Moussa, Srivastava, Amit K., Bulte, Jeff WM. Co-Registration of Bioluminescence Tomography, Computed Tomography, and Magnetic Resonance Imaging for Multimodal In Vivo Stem Cell Tracking. Tomography. 2016; 2(2):159–165. DOI: 10.18383/j.tom.2016.00160 [PubMed: 27478872]

Dutz, Silvio, Hergt, Rudolf. Magnetic particle hyperthermia–a promising tumour therapy? Nanotechnology. 2014; 25(45):452001. doi:10. 1088/0957-4484/25/45/452001. url: http://www.ncbi.nlm.nih.gov/pubmed/25337919. [PubMed: 25337919]

Ferguson, R Matthew, Khandhar, Amit P., Arami, Hamed, Hua, Loc, Hovorka, Ondrej, Krishnan, Kannan M. Tailoring the magnetic and pharmacokinetic properties of iron oxide magnetic particle imaging tracers. Biomedizinische Technik/Biomedical Engineering. 2013; 58(6):493–507. url: http://www.degruyter.com/view/j/bmte.2013.58.issue-6/bmt-2012-0058/bmt-2012-0058.xml. DOI: 10.1515/bmt-2012-0058 [PubMed: 23787461]

Ferguson, R Matthew, Minard, Kevin R., Khandhar, Amit P., Krishnan, Kannan M. Optimizing magnetite nanoparticles for mass sensitivity in magnetic particle imaging. Medical physics. 2011; 38(3):1619–1626. [PubMed: 21520874]

Ferguson, R Matthew, Khandhar, Amit P., Kemp, Scott J., Arami, Hamed, Saritas, Emine U., Croft, Laura R., Konkle, Justin J., Goodwill, Patrick W., Halkola, Aleksi, Rahmer, Jürgen, et al. Magnetic particle imaging with tailored iron oxide nanoparticle tracers. IEEE transactions on medical imaging. 2015; 34(5):1077–1084. [PubMed: 25438306]

Gleich, Bernhard, Weizenecker, Jürgen. Tomographic imaging using the nonlinear response of magnetic particles. Nature. 2005; 435(7046):1214–1217. url: http://www.ncbi.nlm.nih.gov/pubmed/15988521%20http://www.nature.com/doifinder/10.1038/nature03808. DOI: 10.1038/nature03808 [PubMed: 15988521]

Goodwill, Patrick W., Conolly, Steven M. The X-space formulation of the magnetic particle imaging process: 1-D signal, resolution, bandwidth, SNR, SAR, and magnetostimulation. IEEE transactions on medical imaging. 2010; 29(11):1851–9. url: http://www.ncbi.nlm.nih.gov/pubmed/20529726. DOI: 10.1109/TMI.2010.2052284 [PubMed: 20529726]

Goodwill, Patrick W., Conolly, Steven M. Multidimensional X-Space Magnetic Particle Imaging. IEEE Transactions on Medical Imaging. 2011; 30(9):1581–1590. doi:10. 1109/TMI.2011.2125982. [PubMed: 21402508]

Goodwill, Patrick W., Saritas, Emine U., Croft, Laura R., Kim, Tyson N., Krishnan, Kannan M., Schaffer, David V., Conolly, Steven M. X-Space MPI: Magnetic Nanoparticles for Safe Medical Imaging. Advanced Materials. 2012; 24(28):3870–3877. url: http://dx.doi.org/10.1002/adma.201200221. DOI: 10.1002/adma.201200221 [PubMed: 22988557]

Goodwill, Patrick W., et al. In Vivo and Ex vivo experimental MPI angiography with high selection field strength and tailored SPIO nanoparticles; 2015 5th International Workshop on Magnetic Particle Imaging (IWMPI) IEEE. 2015. p. 1-1.url: http://ieeexplore.ieee.org/xpl/articleDetails.jsp?arnumber=7106988%7B%5C&%7Dfilter%7B%5C%%7D3DAND%7B%5C%%7D28p%7B

%5C_%7DIS%7B%5C_%7DNumber%7B%5C%%7D3A7106981%7B%5C%%7D29%20http://ieeexplore.ieee.org/lpdocs/epic03/wrapper.htm?arnumber=7106988

Gu, Luo, Fang, Ronnie H., Sailor, Michael J., Park, Ji Ho. In vivo clearance and toxicity of monodisperse iron oxide nanocrystals. ACS Nano. 2012; 6(6):4947–4954. DOI: 10.1021/nn300456z [PubMed: 22646927]

Hensley D, Goodwill PW, Croft LR, Conolly SM. Preliminary experimental X-space color MPI. Magnetic Particle Imaging (IWMPI), 2015 5th International Workshop on. 2015; :1–1. DOI: 10.1109/IWMPI.2015.7106993

Hergt, Rudolf, Dutz, Silvio, Müller, Robert, Zeisberger, Matthias. Magnetic particle hyperthermia: nanoparticle magnetism and materials development for cancer therapy. Journal of Physics: Condensed Matter. 2006; 18(38):S2919–S2934. DOI: 10.1088/0953-8984/18/38/S26

Janib, Siti M., Moses, Ara S., MacKay, J Andrew. Advanced Drug Delivery Reviews. Vol. 62. Development of Theranostic Agents that Co-Deliver Therapeutic and Imaging Agents; 2010. Imaging and drug delivery using theranostic nanoparticles; p. 1052-1063.doi: http://dx.doi.org/10.1016/j.addr.2010.08.004 url: http://www.sciencedirect.com/science/article/pii/S0169409X10001705

Jokerst, Jesse V., Lobovkina, Tatsiana, Zare, Richard N., Gambhir, Sanjiv S. Nanoparticle PEGylation for imaging and therapy. Nanomedicine (London, England). 2011; 6(4):715–728. url: http://www.ncbi.nlm.nih.gov/pmc/articles/PMC3217316/. DOI: 10.2217/nnm.11.19

Kemp, Scott J., Ferguson, R Matthew, Khandhar, Amit P., Krishnan, Kannan M. Monodisperse magnetite nanoparticles with nearly ideal saturation magnetization. RSC Advances. 2016; 6(81): 77452–77464.

Konkle, Justin J., Goodwill, Patrick W., Lustig, Michael, Lu, Kuan, Conolly, Steven M. X-space Image Reconstruction Algorithm with Optimized 2D/3D DC Recovery. Magnetic Particle Imaging (IWMPI), 2014 4th International Workshop on. 2014:1–1.

Lawaczeck R, Bauer H, Frenzel T, Hasegawa M, Ito Y, Kito K, Miwa N, Tsutsui H, Vogler H, Weinmann HJ. Magnetic iron oxide particles coated with carboxydextran for parenteral administration and liver contrasting. Pre-clinical profile of SH U555A. Acta radiologica (Stockholm, Sweden : 1987). 1997; 38(4 Pt 1):584–97. url: http://www.ncbi.nlm.nih.gov/pubmed/9240682.

Li, Shihong, Goins, Beth, Zhang, Lujun, Bao, Ande. Novel multifunctional theranostic liposome drug delivery system: Construction, characterization, and multimodality MR, near-infrared fluorescent, and nuclear imaging. Bioconjugate Chemistry. 2012; 23(6):1322–1332. arXiv: NIHMS150003. DOI: 10.1021/bc300175d [PubMed: 22577859]

Lu, Kuan, Goodwill, Patrick W., Saritas, Emine U., Zheng, Bo, Conolly, Steven M. Linearity and Shift Invariance for Quantitative Magnetic Particle Imaging. IEEE Transactions on Medical Imaging. 2013; 32(9):1565–1575. DOI: 10.1109/TMI.2013.2257177 [PubMed: 23568496]

Lu, Kuan, Goodwill, Patrick W., Zheng, Bo, Conolly, Steven M. Reshaping the 2D MPI PSF to be isotropic and sharp using vector acquisition and equalization. Magnetic Particle Imaging (IWMPI), 2015 5th International Workshop on. 2015; :1–1. DOI: 10.1109/IWMPI.2015.7106994

Lüdtke-Buzug K, Biederer S, Sattel TF, Knopp T, Buzug TM. Particle-size distribution of dextran- and carboxydextran-coated superparamagnetic nanoparticles for magnetic particle imaging. IFMBE Proceedings. 2009; 25(8):226–229. DOI: 10.1007/978-3-642-03887-7-63

Maeda, Hiroshi, Nakamura, Hideaki, Fang, Jun. The EPR effect for macromolecular drug delivery to solid tumors: Improvement of tumor uptake, lowering of systemic toxicity, and distinct tumor imaging in vivo. Advanced Drug Delivery Reviews. 2013; 65(1):71–79. doi:10.1016/j.addr.2012.10.002. url: http://dx.doi.org/10.1016/j.addr.2012.10.002. [PubMed: 23088862]

Mahmoudi M, Hofmann H, Rothen-Rutishauser B, Petri-Fink A. Assessing the in vitro and in vivo toxicity of superparamagnetic iron oxide nanoparticles. Chem Rev. 2012; 112(4):2323–2338. doi: 10. 1021/cr2002596. url: http://www.ncbi.nlm.nih.gov/pubmed/22216932. [PubMed: 22216932]

Nguyen, Patricia K., Riegler, Johannes, Wu, Joseph C. Stem cell imaging: From bench to bedside. Cell Stem Cell. 2014; 14(4):431–444. arXiv: NIHMS150003. url: http://dx.doi.org/10.1016/j.stem.2014.03.009. DOI: 10.1016/j.stem.2014.03.009 [PubMed: 24702995]

O'Callaghan C, Barry PW. The science of nebulised drug delivery. Thorax. 1997; 52(2):S31–S44. DOI: 10.1136/thx.52.2008.S31 [PubMed: 9155849]

Orendorff, Ryan, Wendland, Michael, Yu, Elaine, Zheng, Bo, Goodwill, Patrick W., Conolly, Steven M. 2016 World Molecular Imaging Congress (WMIC 2016): Imaging Biology… Improving Therapy. World Molecular Imaging Society (WMIS); 2016. First in vivo Brain Perfusion Imaging using Magnetic Particle Imaging.

Rahmer J, Antonelli A, Sfara C, Tiemann B, Gleich B, Magnani M, Weizenecker J, Borgert J. Nanoparticle encapsulation in red blood cells enables blood-pool magnetic particle imaging hours after injection. Physics in medicine and biology. 2013; 58(12):3965–77. url: http://www.ncbi.nlm.nih.gov/pubmed/23685712. DOI: 10.1088/0031-9155/58/12/3965 [PubMed: 23685712]

Rahmer J, Halkola A, Gleich B, Schmale I, Borgert J. First experimental evidence of the feasibility of multi-color magnetic particle imaging. Physics in Medicine and Biology. 2015; 60(5):1775. url: http://stacks.iop.org/0031-9155/60/i=5/a=1775. [PubMed: 25658130]

Ruangwattanapaisarn, Nichanan, Hsiao, Albert, Vasanawala, Shreyas S. Ferumoxytol as an off-label contrast agent in body 3T MR angiography: a pilot study in children. Pediatric Radiology. 2015; 45(6):831–839. arXiv: 15334406. url: http://link.springer.com/10.1007/s00247-014-3226-3. DOI: 10.1007/s00247-014-3226-3 [PubMed: 25427433]

Saritas, Emine U., Goodwill, Patrick W., Croft, Laura R., Konkle, Justin J., Lu, Kuan, Zheng, Bo, Conolly, Steven M. Magnetic Particle Imaging (MPI) for NMR and MRI researchers. Journal of Magnetic Resonance. 2013; 229:116–126. url: http://dx.doi.org/10.1016/j.jmr.2012.11.029%20http://linkinghub.elsevier.com/retrieve/pii/S1090780712003734. DOI: 10.1016/j.jmr.2012.11.029 [PubMed: 23305842]

Shinkai, Masashige. Functional magnetic particles for medical application. Journal of Bioscience and Bioengineering. 2002; 94(6):606–613. DOI: 10.1016/S1389-1723(02)80202-X [PubMed: 16233357]

Wang, Qi, Shen, Ming, Zhao, Tao, Xu, Yuanyuan, Lin, Jiang, Duan, Yourong, Gu, Hongchen. Low toxicity and long circulation time of Polyampholyte-coated magnetic nanoparticles for blood pool contrast agents. Scientific Reports. 2015; 5:7774. url: http://dx.doi.org/10.1038/srep07774%20http://10.1038/srep07774. [PubMed: 25585607]

Wang, Yi-Xiang J. Superparamagnetic iron oxide based MRI contrast agents: Current status of clinical application. Quantitative Imaging in Medicine and Surgery. 2011; 1(1):35–40. url: http://www.ncbi.nlm.nih.gov/pmc/articles/PMC3496483/. DOI: 10.3978/j.issn.2223-4292.2011.08.03 [PubMed: 23256052]

Yu, Elaine, Bishop, Mindy, Zheng, Bo, Ferguson, R Matthew, Khandhar, Amit P., Kemp, Scott J., Krishnan, Kannan M., Goodwill, Patrick W., Conolly, Steven M. 2016 World Molecular Imaging Congress (WMIC 2016): Imaging Biology… Improving Therapy. World Molecular Imaging Society (WMIS); 2016. First demonstration of in vivo Cancer Magnetic Particle Imaging with IV-administered Passive Long-circulating SPIOs.

Zheng, Bo, Vazin, Tandis, Goodwill, Patrick W., Conway, Anthony, Verma, Aradhana, Saritas, Emine U., Schaffer, David V., Conolly, Steven M. Magnetic Particle Imaging tracks the long-term fate of in vivo neural cell implants with high image contrast. Scientific Reports. 2015; 5:14055. url: http://www.nature.com/articles/srep14055. doi: 10.1038/srep14055 [PubMed: 26358296]

Zheng, Bo, von See, Marc P., Yu, Elaine, Gunel, Beliz, Lu, Kuan, Vazin, Tandis, Schaffer, David V., Goodwill, Patrick W., Conolly, Steven M. Quantitative Magnetic Particle Imaging Monitors the Transplantation, Biodistribution, and Clearance of Stem Cells In Vivo. Theranostics. 2016; 6(3):291–301. url: http://thno.org/v06p0291. DOI: 10.7150/thno.13728 [PubMed: 26909106]

Zhou, Xinyi, Yu, Elaine, Keselman, Paul, Goodwill, Patrick W., Nahid, Payam, Zheng, Bo, Conolly, Steven M. 2016 World Molecular Imaging Congress (WMIC 2016): Imaging Biology… Improving Therapy. World Molecular Imaging Society (WMIS); 2016. In Vivo Magnetic Particle Imaging of Lung Perfusion in Rats - Towards High Sensitivity and High Contrast Non-Radiation Based Diagnostics for Pulmonary Embolism.

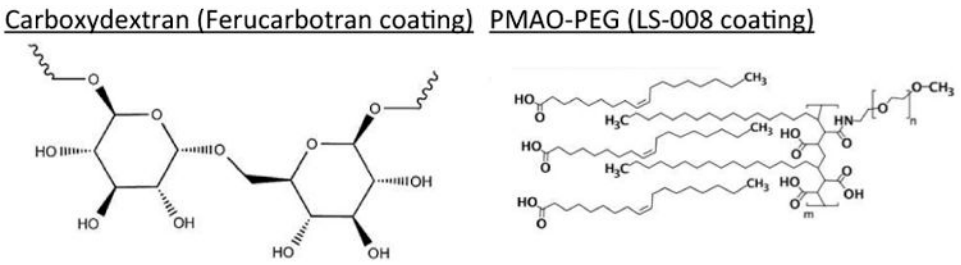

Figure 1.
Chemical diagrams of the tracer coatings.

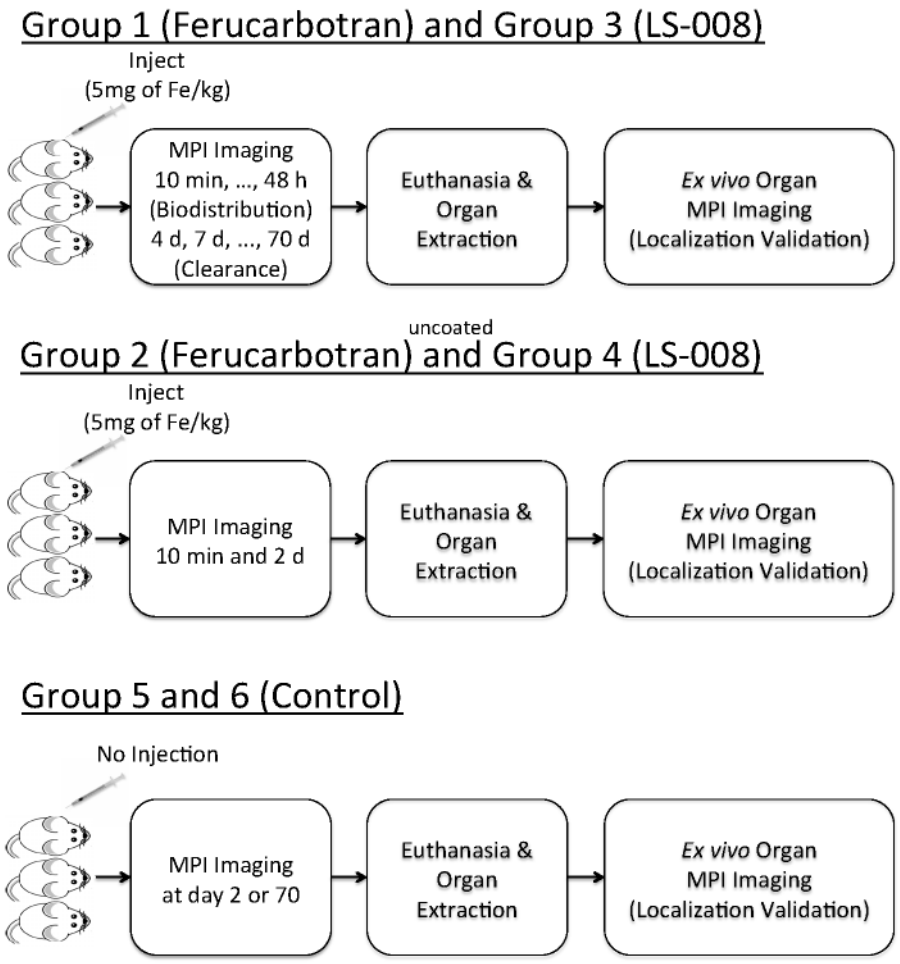

Figure 2.
Flowchart of the tracer biodistribution and long-term clearance animal experiment.

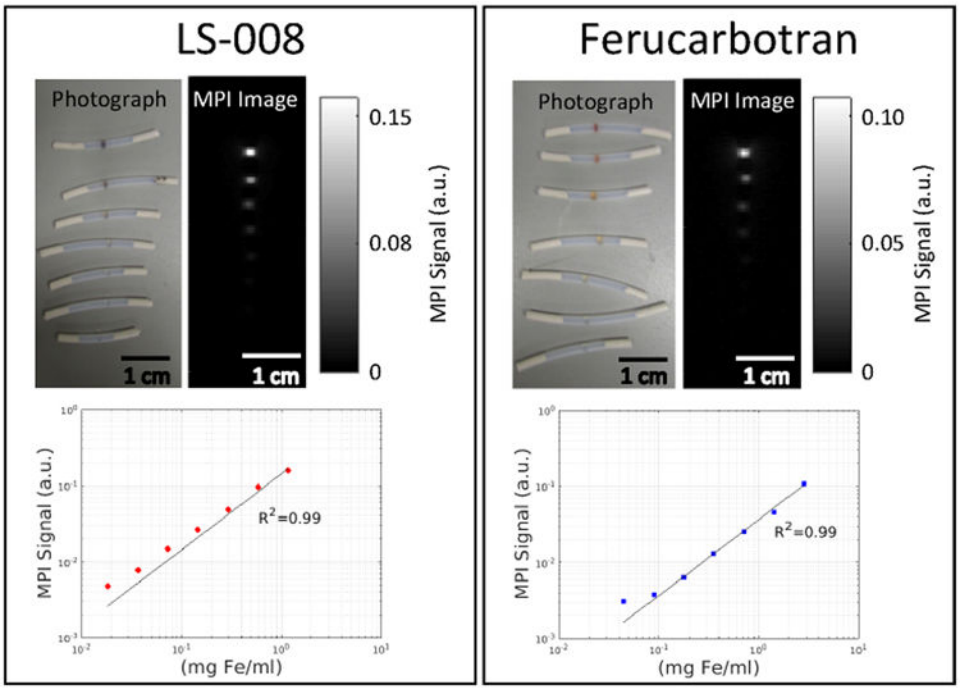

Figure 3.

A series of dilutions were performed to demonstrate the linearity of MPI signal with particle concentration. On the left is a photograph of LS-008 point sources and the corresponding maximum projection intensity MPI image as well as the plot of MPI signal versus Fe concentration. On the right is a photograph of Ferucarbotran point sources and the corresponding maximum projection intensity MPI image as well as the plot of MPI signal versus Fe concentration. In both cases the MPI signal is linear with Fe concentration.

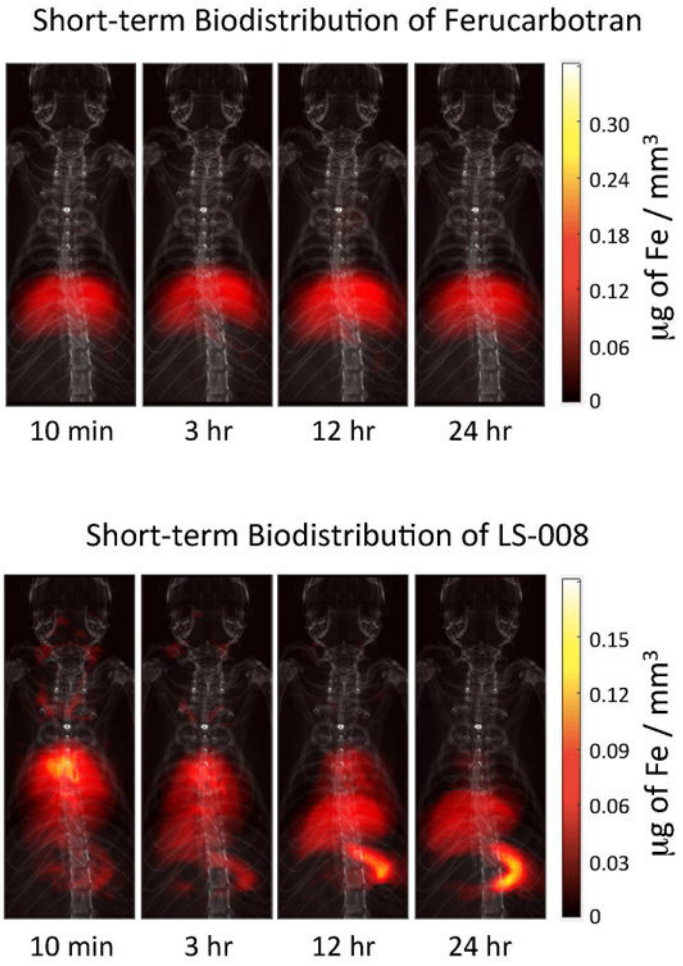

Figure 4.

Short-term biodistribution of Ferucarbotran (top) and LS-008 (bottom) at 4 time points as seen in MPI (dose: 5 mg of Fe / kg for both tracers). The MPI images were overlaid onto projection X-ray images for anatomical reference. In both sets of images the tracer immediately begins to clear to the liver and spleen. For LS-008 tracer, in addition the liver and spleen, we can see what are probably the jugular veins as well as the lungs and heart of the animal. Unlike Ferucarbotran that was designed to immediately clear to the liver, LS-008 stays in circulation. The drastic difference in biodistribution for the two tracers is clearly captured by MPI.

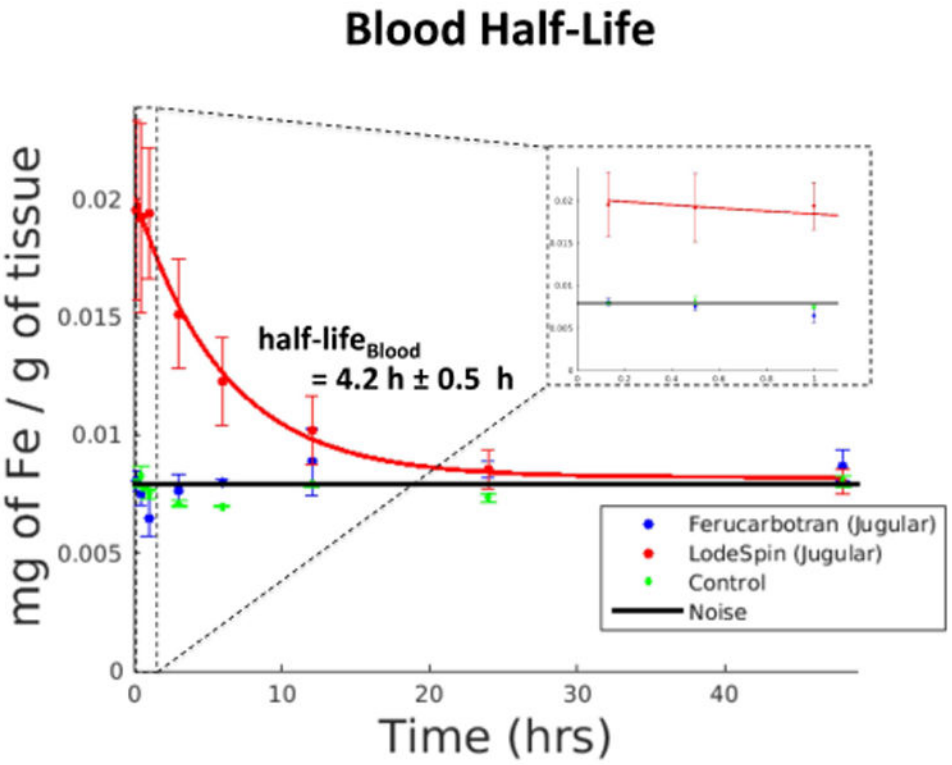

Figure 5.

Average MPI signal in the ROI over the jugular vein of a rats (n = 3) injected with Ferucarbotran, rats (n = 3) injected with LS-008 and rats (n = 3) not injected with anything showing short-term tracer clearance from blood. For rats injected with Ferucarbotran and control rats no discernible jugular vein could be seen in the image so a large box was drawn over the region where jugular vein was estimated to be from the corresponding X-Ray image. The interference noise is an average signal in an ROI drawn over a region outside the body. As expected, LS-008 stays in the blood (half-life 4.2 h ± 0.5 h), while Ferucarbotran is almost immediately cleared to the liver. There is no detectable signal from the control animals. The inset within the dashed line is the data collected during the 1st hour.

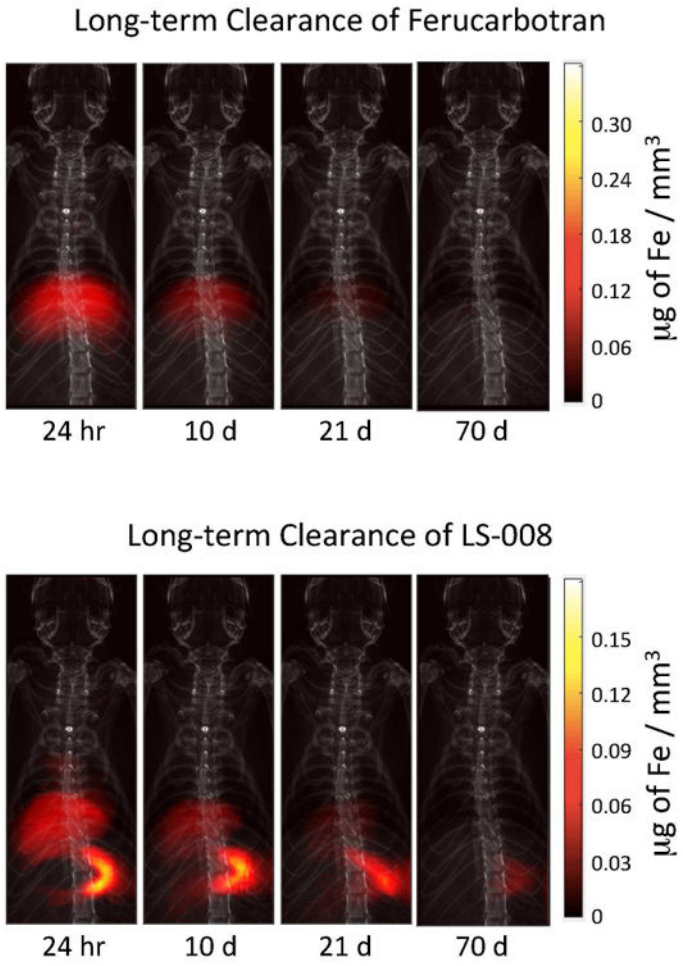

Figure 6.

MPI images of rats injected with Ferucarbotran (top) and LS-008 (bottom) overlaid onto projection X-ray images for anatomical reference. Both tracers were injected at a dose of 5 mg of Fe / kg. MPI images show slow clearance of the tracer by the liver and spleen of a rat over a 70 day period. Ferucarbotran is predominantly cleared by the liver, while Ls-008 is predominantly cleared by the spleen.

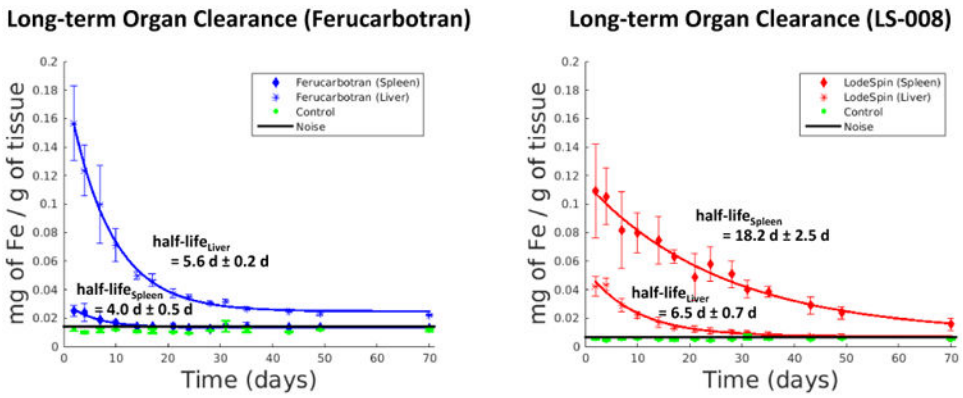

Figure 7.

(left) Long-term clearance of Ferucarbotran from the liver (half-life of 5.6 d ± 0.2 d) and the spleen (half-life of 4.0 d ± 0.5 d) of a group of rats (n=3). (right) Long-term clearance of LS-008 from the liver (half-life of 6.5 d ± 0.7 d) and the spleen (half-life of 18.2 d ± 2.5 d) or a group of rats (n=3). No signal above the interference noise floor was detected from the control animals.

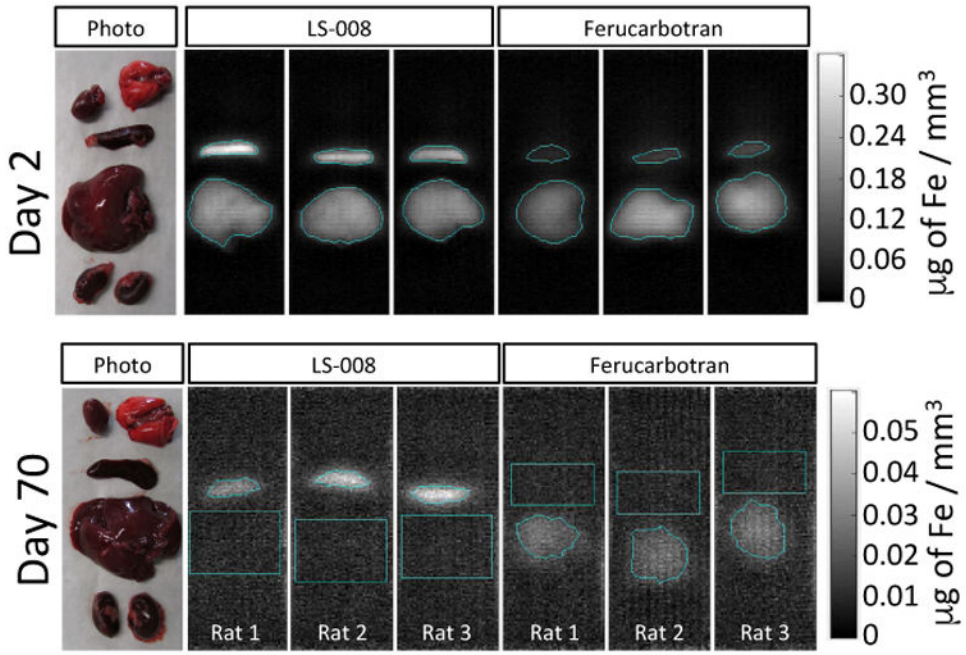

Figure 8.

Top panel shows a representative photograph of the *ex vivo* set-up with the Day 2 excised liver, spleen, kidneys, lungs and heart followed by MPI images of the Day 2 extracted organs for all animals injected with LS-008 and Ferucarbotran. The bottom panel is a similar photograph and MPI image of organs extracted at day 70 after the injection. At day 70, LS-008 signal is only observed in the spleen and Ferucarbotran signal is only observed in the liver.

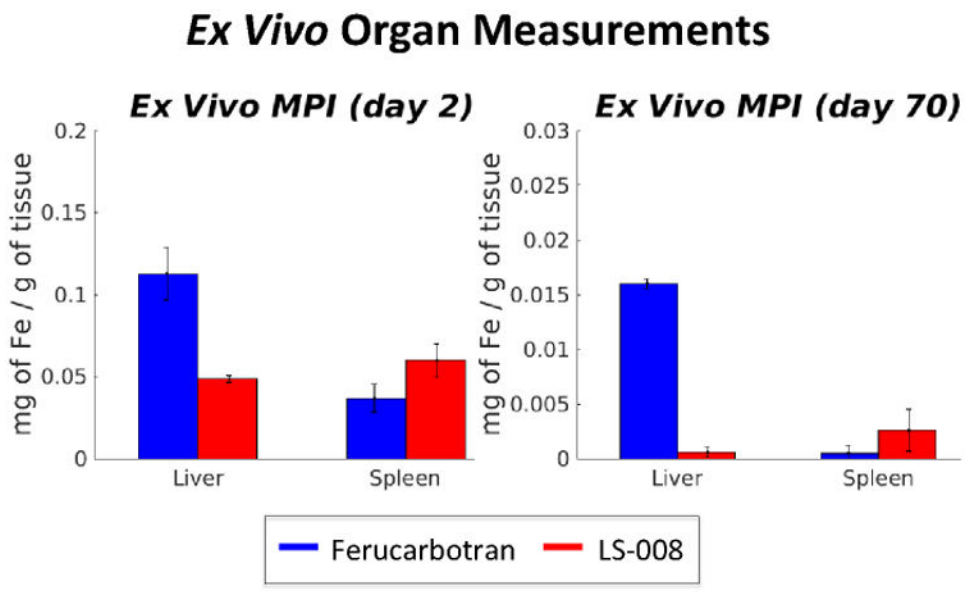

Figure 9.

Ex vivo Organ measurements for Ferucarbotran and LS-008 at day 2 and day 70. As with *in vivo* data, LS-008 is cleared predominately through the spleen, while Ferucarbotran is cleared through the liver. No signal was seen in the heart, lungs or kidneys. And no signal was detected in the organs of the control animals.

Table 1

Summary of Ferucarbotran and LS-008 Trace Characteristics.

Name	Ferucarbotran	LS-008
Supplier	Meito Sangyo Co., Japan	LodeSpin Labs, Seattle WA
Coating	Carboxydextran	PMAO-PEG
Core Diameter	3 nm to 5 nm	26.3 nm ± 1.5 nm
Hydrodynamic Diameter	45 nm to 72 nm	78 nm
Concentration of Iron (Fe)	5.7 mg/ml	2.35 mg/ml